IFAC Control Engineering Practice 8 (2000) 985--1001

Parameter identification for inflight detection and characterization of aircraft icing*

J. W. Melody T. Başar W. R. Perkins
P. G. Voulgaris
Coordinated Science Laboratory, University of Illinois
1308 West Main Street
Urbana, IL 61801-2307 / USA

Abstract

Increasing interest in aircraft icing has motivated the proposal of a new ice management system that would provide inflight monitoring of ice accretion effects. Since these effects are manifested in the flight dynamics, parameter identification is a critical element of ice detection. In particular, identification must provide timely and accurate parameter estimates under normal operational input in the presence of disturbances and measurement noise. This paper evaluates a batch least-squares algorithm, an extended Kalman filter, and an H^∞ algorithm in the context of icing detection. Simulation results show that only the H^∞ method provides a timely and accurate icing indication.

Key words: Aircraft control; Identification; H-infinity; Kalman Filter; Least squares; Robustness.

1. Introduction

Recently there has been increasing interest in developing aircraft that are more robust to icing and severe weather conditions. This interest is largely driven both by recent and more visible icing accidents (*e.g.*, the American Eagle crash that killed 68 people near Roselawn, Indiana USA, in October 1994) and by the preponderance of icing as the cause of aviation accidents (between 1975 and 1988 there were 803 known icing-related accidents in the USA, with roughly half resulting in fatalities) as reported by Cole & Sands (1991). Recently the National Aeronautics and Space Administration of the United States of America (NASA) has responded to the President's Commission on Aviation Safety and Security to develop a national aviation safety research plan. Aircraft icing was determined to be a high national priority during this process (NAS, 1997).

Aircraft icing accidents result from the effect of ice accretion on the performance, stability, and controllability of the aircraft. In particular, Lee & Bragg (1999) have shown that as ice accretes on

*Preliminary results related to this paper were presented at the 14^{th} IFAC World Congress, Beijing, P. R. China, 5–9 July, 1999. Corresponding Author and mailing address: Prof. T. Başar, Coordinated Science Laboratory, University of Illinois, 1308 West Main Street, Urbana, IL 61801-2307/USA. Tel. (217) 333-3607, Fax. (217) 244-1653, E-mail: tbasar@control.csl.uiuc.edu.

the aircraft flight surfaces, it changes their aerodynamics by modifying both their shape and their surface roughness, typically increasing their drag and decreasing their lift. The particular effect of icing on the aerodynamics of a lift surface is a complicated function as much of the ice shape and location as of the amount of ice. These characteristics in turn depend in a complicated fashion on atmospheric conditions such as the amount, temperature, and droplet size of water in the air (Olsen & Shaw, 1984). The composite effect of this aerodynamic deterioration over all lift surfaces is a degradation of aircraft flight dynamics. In severe atmospheric conditions, dangerous levels of icing can be obtained on the order of tens of minutes. Small to moderate amounts of icing will generally cause a reduction in aircraft performance in terms of climb rates, range, endurance, and maximum speed and acceleration. Icing effects of this type are known as performance events. As icing increases, separation of air flow from the flight surfaces can cause loss of pilot control and even wildly unstable behavior. These more severe icing events, known as handling events, are often precipitated by a change in the aircraft configuration (*e.g.*, flap retraction) or an aircraft maneuver effected by a pilot unaware of the flight dynamics degradation. This was the case in the Roselawn accident where the aircraft experienced an uncontrolled roll of 120° in 5 s after the pilot initiated a flap retraction. Handling events generally can be classified into either tailplane stall, where the aircraft pitches forward, or asymmetric wing effects causing a roll upset as in the Roselawn accident. Two aspects of icing accidents and incidents are particularly of interest: 1) icing is of concern insofar as it affects the aircraft flight dynamics, and 2) icing events can be exacerbated when the pilot takes action while unaware of the severity of these effects.

Current aircraft inflight ice protection systems (IPS) consist of de-icing and anti-icing systems that respectively remove ice or inhibit accretion, as well as stall protection systems that seek to restrict the aircraft to some presumed safe region of operation, or "flight envelope," by limiting pilot input. These current systems use little if any information about the present state of the aircraft performance, stability, or controllability. Oftentimes these systems rely on pilot activation. There are several notable examples of icing accidents occurring on aircraft equipped with ice protection systems, where either the IPS was not activated by the pilot or the IPS was activated but was not effective. The new approach to aircraft icing safety, advanced by Bragg, Perkins, Sarter, Başar, Voulgaris, Gurbacki, Melody & McCray (1998), is to provide both the pilot and the IPS with a near real-time characterization of the effect of ice on the aircraft performance, stability, and controllability. This new approach incorporates parameter identification of the flight dynamics, which is what this paper addresses. Specifically, this paper investigates the performance of three parameter identification schemes, a batch least-squares algorithm, an extended Kalman filter, and a recursive H^∞ algorithm, applied (in simulation) to the flight dynamics of an inflight icing research aircraft, the NASA Twin Otter. The algorithms are evaluated in terms of both parameter convergence rate and parameter estimate accuracy in the presence of disturbances and noise, with the ultimate objective of providing a timely characterization of icing.

1.1 Ice management system

As presented by Bragg et al. (1998), the current model of an aircraft icing encounter is depicted in Figure 1. As ice accretes on the aircraft, the ice accretion sensors relay this information to the pilot. In most cases it is up to the pilot to activate the IPS ("advisory system"), although some aircraft have automatic activation ("primary system"). Ice accretion on the flight surfaces negatively affects the flight dynamics. The IPS seeks to reduce this effect by removing accreted

ice. Aside from the pilot/auto-pilot's perception of the input/output response of the system, it has no real-time knowledge of the degradation of the flight dynamics caused by icing. A simple flight envelope protection function may be included with the IPS, such as a reduction in the angle of attack at which the stick shaker engages to notify the pilot of an impending stall (Bragg et al., 1998). Aside from this crude device, the IPS does not provide the pilot/auto-pilot with any sense of the flight dynamics degradation.

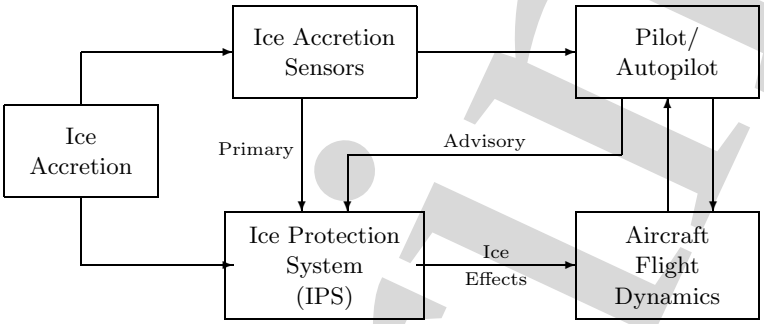

Figure 1: Block diagram of current Ice Protection System (IPS) operation.

The approach that Bragg et al. (1998) have proposed adds another level of safety, an Ice Management System (IMS), as depicted in Figure 2. The IMS monitors the ice accretion and its effects, and assists the pilot/auto-pilot in safe operation of the aircraft in the iced state. The IMS provides three functions: 1) sense the presence of ice accretion and its effect on the flight dynamics; 2) activate and manage the IPS and provide the pilot with a characterization of the icing effects; and 3) modify the flight envelope in order to maintain safe operation. To accomplish these functions, the IMS will receive input from the ice sensors, the IPS system, the flight crew, and flight dynamics measurements.

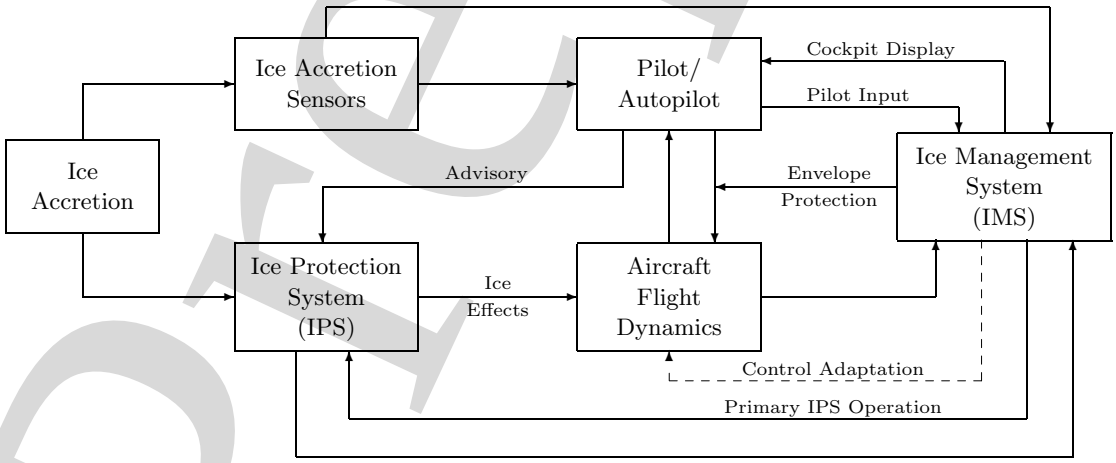

Figure 2: Proposed addition of Ice Management System (IMS) (Bragg et al., 1998).

As an additional level of safety, control adaptation could be added to maintain acceptable flying qualities during a performance icing event. Reconfiguring the control laws would enable the

pilot/auto-pilot to maintain control of the aircraft within some limited flight envelope until the icing conditions could be exited safely. In the worst contingency, adaptive control could be used to stabilize the aircraft after the onset of a handling event.

1.2 Ice characterization methodology

Essential to reliable operation of the IMS are the development and testing of appropriate identification algorithms. It is not sufficient to rely merely on icing sensors, since they may not be generally available or cost effective on many aircraft, particularly commuter aircraft which are more sensitive to icing. More importantly, the complex relation between flight dynamics effects on the one hand and ice shape and location on the other makes characterization of icing effects based on ice sensors difficult. Another method for icing characterization is to use force-balance relations in steady, level flight (*i.e.*, thrust = drag and lift = weight) to detect an icing event. The addition of acceleration measurements would enable a similar technique during maneuver. Bragg et al. (1998) have reported that ice accretion can cause an increase in drag of up to several hundred percent. Similarly, Bragg (1996) has demonstrated that ice accretion can be correlated to an increase in aerodynamic hinge moments. Indeed, these correlations are being pursued as possible means of detecting ice accretion as part of the IMS. However, steady-state drag and lift characterization and hinge moment measurements will most likely not be effective in providing a characterization of the *type* of icing effects. It is identification of the flight dynamics that gets directly to the heart of the matter: the effect of icing on the flight dynamics.

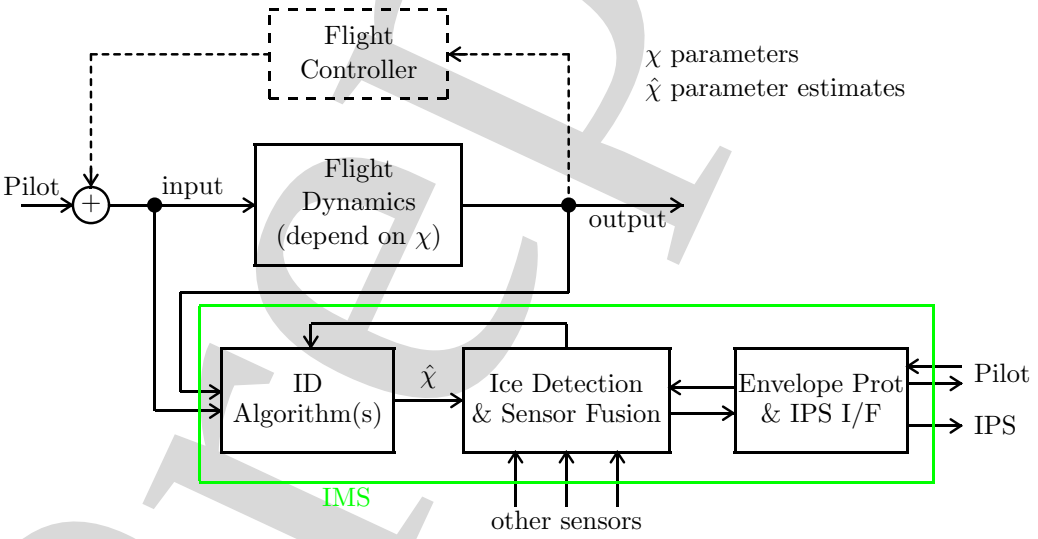

Figure 3: Aircraft icing detection and characterization block diagram.

These identification algorithms must identify aircraft performance, stability, and control parameters over time, based on measurements of the aircraft state variables and control input. It is well known that system excitation is necessary for identification. Generally speaking, input with larger amplitude and richer frequency content results in more accurate identification. Often in identification applications, a test input is introduced to facilitate the identification. However, in

this case it is assumed that test excitation input for the purpose of identification is not acceptable, and hence the identification process must perform well under excitation due to normal operational maneuvers. Since icing safety problems can occur at any time from takeoff to landing, effective icing characterization must function in all phases of flight.

A block diagram of an icing identification system is shown in Figure 3, which is a detailed representation of the IMS and Aircraft Dynamics blocks of Figure 2. Specifically, the aircraft flight dynamics characterized by some parameters, say χ, are considered. The identification algorithm seeks to identify these parameters by observing the system input and output, and calculating a parameter estimate, $\hat{\chi}$, based on this available information. Since ice accretion will cause variations in the system parameters, on-line estimation of these parameters provides information on the degradation due to ice accretion. The IMS makes use of detection criteria applied to the parameter estimates both to trigger an indicator for the presence of icing, and to classify the icing type and severity. In addition, the IMS incorporates other available and pertinent sensor information, such as aerodynamic measurements, ice sensors, and steady-state characterization, into the icing characterization. One possible implementation of this sensor fusion and characterization function is a neural network. Preliminary results for neural network detection and classification of icing based on parameter estimates alone have been obtained by Schuchard, Melody, Başar, Perkins & Voulgaris (2000). A positive indication of icing can result in modification of the flight envelope based on the characterization of the icing effects, notification of the pilot, and/or adaptation of the flight control system.

The identification algorithm to be developed for this purpose must be able to address both performance icing events and handling icing events. For the former, the identification algorithm must sense small changes in the flight dynamics under normal (*i.e.*, relatively small) levels of excitation, and hence it is natural here to consider a linearized version of the flight dynamics. For the latter, since handling events generally involve large excursions of the aircraft state, the algorithm should be robust to the effect of the nonlinearity in the flight dynamics and should be able to quickly sense large changes in the flight dynamics. Even so, it is generally thought that every handling event is preceded by a performance event. Hence, both types of events can be addressed by early detection and characterization of performance icing effects. However, since the precise boundary between handling and performance events is not well understood, and since a performance event can become a handling event through the actions of an unsuspecting pilot at any time, identification during performance events should be robust to nonlinearities in the flight dynamics. This study addresses parameter identification for characterization of performance icing events during a maneuver such as takeoff or landing approach since icing during these periods of flight is generally more dangerous. Parameter identification for detection and characterization of performance events during steady-level flight based on excitation due to turbulence alone is also possible, as preliminary results of Hillbrand (1999) demonstrate.

Research strongly related to the approach discussed above has been conducted in the context of adaptation, or "reconfiguration," of the flight control systems of fighter aircraft (Chandler, Pachter & Mears, 1995; Ward & Barron, 1995). In particular, current research efforts related to the new generation of tailless fighters are focused on the identification of flight dynamics parameters when sudden changes due to failure or battle damage occur. The identified parameters are used to adjust the flight control laws in an attempt to maintain the aircraft's stability and handling qualities. Results using linear and nonlinear models and static modified least-squares algorithms, along with the adaptation of inversion control laws, are encouraging. Recent research, as reported by Chandler

et al. (1995) and Ward & Barron (1995), has described both the parameter ID algorithms as well as their successful application to control reconfiguration. They also consider various important issues such as the tradeoff between using recursive least squares algorithms and using static algorithms operating on a window of data. Moreover, they discuss the issues associated with turning off the ID algorithm when insufficient excitation is present, and the detection of a damage event (*i.e.*, parameter jumps) within a window of data.

The icing study is similar to these reconfiguration studies in that it also entails identifying flight dynamics parameters and using these identified parameters to detect and characterize changes in the flight dynamics. Furthermore, the icing study may also ultimately combine the parameter identification with control adaptation. However, with icing detection both the parameter variations and the excitation are usually small, whereas with fighter aircraft control reconfiguration the parameter changes are abrupt. Hence parameter changes for fighter aircraft control reconfiguration are easier to recognize. Furthermore, excitation is generally larger for fighter aircraft in battle situations than for commercial aircraft. This study must focus on parameter convergence rates in the presence of smaller excitation. Of course, the controllability requirements for commercial aircraft are less demanding.

2. Flight dynamics model

Simply put, flight dynamics describe the motion of the aircraft in response to pilot input and external disturbances. Ignoring flexibility in the airframe, the aircraft motion is described by translations and rotations of a rigid body in space, acted on by aerodynamic, gravitational, and propulsive forces and torques. The six degree-of-freedom motion of a rigid body is well understood, and can be described in a number of ways, depending on the adopted coordinate system, *e.g.*, Euler angles, quaternions, or more abstractly the Lie group $SE(3)$ (Murray, Sastry & Li, 1994). This rigid-body motion, even without any external forces or moments, is nonlinear due to gyroscopic coupling effects. Similarly, the gravitational forces are easily described. The difficulty is in modeling the aerodynamic, and to a lesser extent, the propulsive forces and torques, since these depend in a nonlinear and complex manner on the aircraft state and even in some cases on the state derivative (see Etkin & Reid, 1996). Indeed, a rich area of research in computational fluid dynamics is the determination of aerodynamic forces and torques acting on an aircraft. When this nonlinear nature of aerodynamic forces is incorporated into a flight dynamics model (*e.g.*, in flight simulators) it is generally modeled via look-up tables (Stevens & Lewis, 1992). Since detection and characterization of performance events during relatively small excursion maneuvers are addressed, it is reasonable to adopt a linearized flight dynamics model.

The typical simplification is to linearize the flight dynamics about an operating point, or "trim condition," via Taylor series expansion, and to determine the values of the first-order partial derivatives via either numerical simulation, wind tunnel measurements, or flight tests (Roskam, 1982). (This "Taylor series expansion" is a slight abuse of terminology, since most references never write an explicit nonlinear relation for the aerodynamic forces, but instead write the linear flight dynamics parameterized by "derivatives," thus implicitly linearizing the system without ever actually taking a partial derivative.) Within this linear framework there is a natural decoupling of the flight dynamics into longitudinal and lateral dynamics. As shown in Figure 4, longitudinal dynamics describe the three degree-of-freedom motion of forward translation, vertical translation, and pitching (*i.e.*, nose forward rotation). Lateral motion comprises sideways translation, roll rotation, and

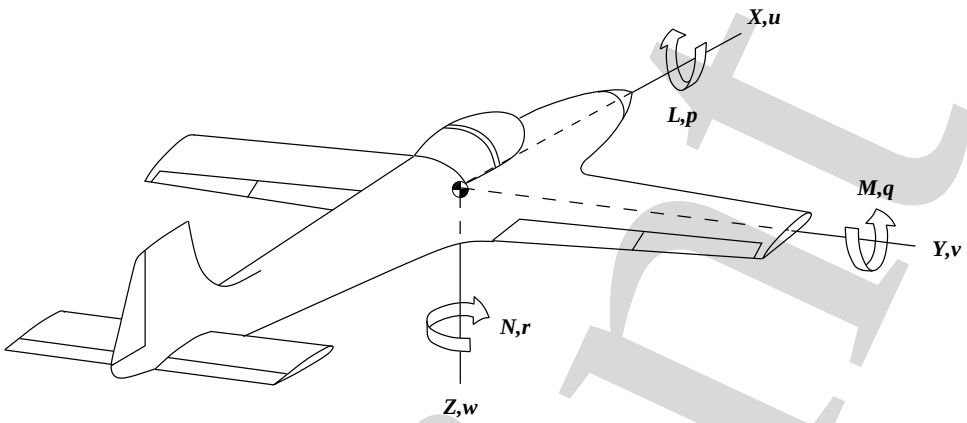

Figure 4: Aircraft flight dynamics decomposition. Longitudinal dynamics comprise translation along the x- and y-axes, as well as rotation about the z-axis (pitch). Lateral flight dynamics comprise translation along the z-axis, as well as rotation about the x-axis (roll) and about the y-axis (yaw).

twisting, generally called yaw. In general, tailplane icing affects primarily (though not exclusively) the longitudinal dynamics, whereas wing icing affects primarily the lateral dynamics. Since the flight dynamics model discussed herein is based on the tailplane icing research of the NASA Twin Otter reported by Ratvasky, Van Zante & Riley (1999), only the longitudinal flight dynamics are considered. Using the notation of Roskam (1982), but including explicitly the nonlinear terms that are ignored under the small perturbation assumption, the longitudinal flight dynamics are

$$\dot{u} = -g\theta\cos(\Theta_\circ) + (X_u + X_{T_u})u + X_\alpha\alpha + X_{\delta_E}\delta_E + f_u + \dot{u}_w \tag{1}$$

$$\dot{w} = -g\theta\sin(\Theta_\circ) + Z_u u + Z_\alpha\alpha + Z_{\dot{\alpha}}\dot{\alpha} + Z_{\delta_E}\delta_E + (Z_q + U_\circ)q + f_w + \dot{w}_w \tag{2}$$

$$\dot{q} = (M_u + M_{T_u})u + (M_\alpha + M_{T_\alpha})\alpha + M_{\dot{\alpha}}\dot{\alpha} + M_q q + M_{\delta_E}\delta_E + f_q \tag{3}$$

where u is the forward velocity perturbation, w is the downward velocity perturbation, q is the pitch rate perturbation, θ is the pitch angle perturbation, α is the angle of attack perturbation, and δ_E is the elevator deflection angle perturbation controlled by the pilot. $U_\circ$ and $\Theta_\circ$ represent the trim condition values of forward velocity and pitch angle, respectively. Wind turbulence is modeled as perturbations to the vertical and horizontal acceleration, represented by the terms $\dot{u}_w$ and $\dot{w}_w$, respectively. f_* are poorly-known nonlinear functions of both the longitudinal and lateral dynamics state and state derivative that represent the nonlinearity of the flight dynamics. The essence of linearization is that these nonlinear terms vanish in a well-behaved fashion at the trim condition, and hence as the state perturbations get small, the behavior of the true nonlinear system approaches that of the linearized system (see for example Khalil (1996) for a detailed discussion of linearization). The flight dynamics nonlinearities are included explicitly for several reasons: 1) a severely iced aircraft could be near instability, and hence could move away from the linearization point substantially even under small excitation, 2) icing conditions are thought to be somewhat correlated with heavy turbulence conditions which might cause the nonlinear effects to become significant, and 3) ultimately this parameter identification may be coupled with adaptive control techniques that would seek to stabilize the aircraft in the event of a handling event, which by definition entails large excursions of the aircraft state.

The coefficients M_*, Z_*, and X_* in (1)–(3), are known as "stability" or "control" derivatives, as appropriate. The effects of icing are manifested in changes in these stability and control derivatives, as well as in changes in the nonlinearities represented by the functions f_*. During an icing encounter, the stability and control derivatives will change slowly over a period of several minutes. However, since investigating identification during a maneuver that will last several seconds only is investigated, a constant (but unknown) parameter model of the flight dynamics is considered.

As mentioned above, for this study the NASA Twin Otter inflight icing research aircraft has been adopted as a model. This decision will ultimately allow validation of the developed icing detection methodology with actual flight measurements. Stability and control derivatives for the clean and iced-tailplane aircraft are calculated from the results reported by Ratvasky & Ranaudo (1993). The iced aircraft model corresponds to a severely iced tailplane condition. From these results, it was determined that the only significant variations occur in the M_α, M_q, Z_α, Z_q, X_α and $(X_u + X_{T_u})$ stability derivatives, and in the M_{δ_E} and Z_{δ_E} control derivatives. Hence, these are the parameters to be identified. The values for the parameters under clean and iced conditions are given in Table 1.

Table 1: Values of stability and control derivatives of the NASA Twin Otter that are affected by icing. These derivatives constitute the parameter vector χ in (4). Values are given for both the iced and clean conditions.

	M_α	M_{δ_E}	M_q	Z_α	Z_{δ_E}	Z_q	X_α	$X_u + X_{T_u}$
Clean	-7.86	-10.44	-3.055	-378.7	-40.30	-19.70	13.71	-0.018
Iced	-7.08	-9.40	-2.948	-342.7	-36.45	-19.43	13.90	-0.020

The scenario modeled is a period of steady, level flight, during which ice has accreted on the tailplane, followed by a maneuver (*e.g.*, the initiation of a landing approach descent). It is assumed that test excitation input for the purpose of identification is not acceptable, and hence only excitation due to a normal operational maneuver is considered. The baseline maneuver is modeled as a 5° doublet over a period of 10 s (*i.e.*, one period of a sinusoid with frequency 0.1 Hz and amplitude 5°). After the maneuver begins, the parameter ID algorithm provides parameter estimates from which an icing indication may be inferred. The goal is to provide an accurate icing indication within several seconds, before a handling event may be precipitated by the maneuver. Even though icing detection and characterization will ultimately be performed by a sophisticated algorithm that incorporates all pertinent sensor information, in this study the mean of the clean and iced parameters (for each parameter) is used as a detection threshold for easy evaluation and comparison of the various identification algorithms considered.

3. Parameter ID algorithms

For the problem formulated in the previous section, the parameter identification framework of Didinsky, Pan & Başar (1995) is utilized. This framework generally involves a state-space system (possibly nonlinear) which is linear in the parameters, χ, to be identified

$$\dot{x} = A(x, v)\chi + b(x, v) + d_p \tag{4}$$

$$y = x + d_m \tag{5}$$

where $x \in \mathbb{R}^n$ is the system state, $y \in \mathbb{R}^n$ is the measured output, $v \in \mathbb{R}^m$ is the input, $d_p \in \mathbb{R}^n$ is the (unknown) process disturbance, $d_m \in \mathbb{R}^n$ is the measurement noise, and $\chi \in \mathbb{R}^r$ is the parameter vector to be estimated. In general, d_p may be used to represent stochastic or deterministic exogenous input, model inaccuracy, or unmodeled high-frequency or nonlinear dynamics. When the nominal system is also linear in state and input for fixed χ, the functions $A(x,v)$ and $b(x,v)$ are described by the linear matrix relations

$$A(x,v) = [F_1 x + G_1 v \ \cdots \ F_r x + G_r v] \tag{6}$$

$$b(x,v) = [F_\circ x + G_\circ v]\,. \tag{7}$$

The goal is to obtain estimates of the parameters from the available information, that will be accurate in the presence of disturbances, unmodeled dynamics, model inaccuracies, and measurement noise.

With the parameter set specified as $\chi := \mathrm{col}(M_\alpha, M_{\delta_E}, M_q, Z_\alpha, Z_{\delta_E}, Z_q, X_\alpha, X_u + X_{T_u})$, the longitudinal flight dynamics are transformed into the parameter ID formulation (4)–(5) using (6)–(7). This is accomplished by expressing the longitudinal flight dynamics in first-order, state-space form with the state defined as $x = \mathrm{col}(q, \theta, \alpha, u)$, and the input as $v = \delta_E$. Using the (linearized) relation $w = U_\circ \alpha$, the model becomes $\dot{x} = Fx + Gv$ where $G = \left[M_{\delta_E} + \overline{M} Z_{\delta_E} \ \ 0 \ \ Z_{\delta_E}/\overline{U} \ \ X_{\delta_E}\right]^T$, $F = [F^1 \ F^2]$ where

$$F^1 = \begin{bmatrix} M_q + \overline{M}\,(U_\circ + Z_q) & -\overline{M} g \sin(\Theta_\circ) \\ 1 & 0 \\ (U_\circ + Z_q)/\overline{U} & -g\sin(\Theta_\circ)/\overline{U} \\ 0 & -g\cos(\Theta_\circ) \end{bmatrix}$$

and

$$F^2 = \begin{bmatrix} M_\alpha + M_{T_\alpha} + \overline{M} Z_\alpha & M_u + M_{T_u} + \overline{M} Z_u \\ 0 & 0 \\ Z_\alpha/\overline{U} & Z_u/\overline{U} \\ X_\alpha & X_u + X_{T_u} \end{bmatrix},$$

$\overline{M} := M_{\dot{\alpha}}/(U_\circ - Z_{\dot{\alpha}})$, and $\overline{U} := U_\circ - Z_{\dot{\alpha}}$. From these matrices, F_i and G_i are given by

$$F_i = \begin{cases} \dfrac{\partial}{\partial \chi_i} F & \text{for } i = 1, \ldots, r \\ F - \displaystyle\sum_{i=1}^{r} F_i & \text{for } i = 0 \end{cases}$$

and

$$G_i = \begin{cases} \dfrac{\partial}{\partial \chi_i} G & \text{for } i = 1, \ldots, r \\ G - \displaystyle\sum_{i=1}^{r} G_i & \text{for } i = 0. \end{cases}$$

Furthermore, the process noise disturbance d_p is used to represent the turbulence terms $\dot{u}_w$ and $\dot{w}_w$ as well as the unknown nonlinearity of the terms f_*. Since the vertical velocity is represented

in the state x by α, according to $w = U_\circ \alpha$, turbulence enters the dynamics through α as well as through u. Thus, the turbulence portion of d_p is given by $\mathrm{col}(0, 0, \dot{w}_w/U_\circ, \dot{u}_w)$.

The parameter ID algorithm will depend on the type of measurements available. Following Didinsky et al. (1995), this information state is classified into three categories: 1) full-state derivative information (FSDI), where the state, state derivative, and input are known; 2) full-state information (FSI), where only the state and input are known; and 3) noise perturbed full-state information (NPFSI), where the input and a noise perturbed measurement of the state are known. In the case of flight dynamics, perfect measurements of both the state and the state derivative may not be available.

A detailed discussion and classification of parameter and system identification algorithms is both a digression from and beyond the purview of this paper. Many texts address parameter identification in the discrete-time, good examples being Ljung (1999) and Åström & Wittenmark (1995). The more neglected continuous-time case is discussed in Sastry & Bodson (1989). Despite this plethora of algorithms, the needs of icing characterization are more pathological since on the one hand there is a disturbance d_p that cannot be completely characterized stochastically, and on the other hand there is the possibility of nonnegligible nonlinearity. These two difficulties have dictated the consideration of the robust H^∞ identification results of Didinsky et al. (1995), which is a generalization of the well-known recursive least squares (RLS) and least mean squares (LMS) algorithms presented for example in Sastry & Bodson (1989). The static least-squares algorithm used by Chandler et al. (1995) for the fighter aircraft control reconfiguration studies previously mentioned is considered, as the application is similar to inflight icing characterization. Finally, the familiar Kalman filtering technique is applied, since it is commonly used in practice. As opposed to the static algorithm of Chandler et al. (1995), both the H^∞ techniques of Didinsky et al. (1995) and the Kalman filtering techniques are recursive, meaning that the parameter estimate at any given time is a function not just of the information available at that time, but also of all past measurements. These techniques are dynamic in the sense that the identification itself has a state that evolves according to (in this case) differential equations.

3.1 Static and batch least-squares algorithms

In static algorithms the parameter estimate at any instant is dependent on the information available at that instant. Essentially, (4) is treated as a linear system of equations in the unknown parameter χ by disregarding the noise, d_p. Oftentimes, static algorithms are extended by collecting a batch of measurements from various time instants and processing them together. These algorithms, which are referred to as batch algorithms, are implemented in real time by concatenating several previous measurements with the present measurement. Static and batch ID can also be thought of in terms of linear regression where the disturbance $d_p(t)$ is assumed to be a random variable, and the associated covariance is taken into account. It is this linear regression formulation that is implemented for the reconfigurable aircraft control by Chandler et al. (1995).

The algorithm considered is a batch least-squares algorithm where it is not assumed that $d_p(t)$ can be characterized statistically. In particular, the algorithm uses a sliding batch window, where at any time instant t the algorithm will concatenate the previous m measurements taken with sample period T. The period of time over which the measurements are concatenated together, called the batch period and denoted by T_b, is thus mT. At time t, the system of equations will take the form

$$A(x_{t_i}, v_{t_i})\chi = \dot{x}_{t_i} - b(x_{t_i}, v_{t_i}) \tag{8}$$

for $i = 1, \ldots, m$, where $t_i = t - (m-i)T$, and x_{t_i}, $\dot{x}_{t_i}$, and v_{t_i} denote the measurements at time t_i. For the sake of simplification, (8) will be written as

$$\mathcal{A}\chi = \dot{X} - \mathcal{B}. \tag{9}$$

In the FSDI case, $\dot{X}$, $\mathcal{A}$, and $\mathcal{B}$ are known, and the implementation of the algorithm is a matrix least squares solution,

$$\hat{\chi} = \left[\mathcal{A}^T\mathcal{A}\right]^{-1}\mathcal{A}^T\left(\dot{X} - \mathcal{B}\right) \tag{10}$$

where an estimate $\hat{\chi}$ is produced every T seconds. Note that in order for $\mathcal{A}^T\mathcal{A}$ to be invertible, $\mathcal{A}$ must have full column rank. Hence, there must be a sufficient number of measurements, and the system must have sufficient excitation so that the individual equations of (8) have a subset of r linearly independent (scalar) equations.

The parameter estimation error, $\tilde{\chi}$, is given by

$$\tilde{\chi} := \chi - \hat{\chi} = \left[\mathcal{A}^T\mathcal{A}\right]^{-1}\mathcal{A}^T\mathcal{D}_p \tag{11}$$

where $\mathcal{D}_p$ is the concatenation of $d_p(t_1)$, ..., $d_p(t_m)$. Using the fact that the induced Euclidean norm of a matrix is its largest singular value, it is clear from (11) that the disturbance attenuation $|\tilde{\chi}|/|\mathcal{D}_p|$ can be as much as $\bar{\sigma}(\left[\mathcal{A}^T\mathcal{A}\right]^{-1}\mathcal{A}^T)$, where $\bar{\sigma}$ represents the largest singular value. But $\bar{\sigma}(\left[\mathcal{A}^T\mathcal{A}\right]^{-1}\mathcal{A}^T)$ is merely $1/\underline{\sigma}(\mathcal{A})$ where $\underline{\sigma}$ denotes the smallest singular value. Since $\underline{\sigma}(\mathcal{A})$ (for a fixed batch period) varies inversely with the excitation level, the sensitivity of the parameter estimate error to disturbances will depend on that level. On the other hand, the disturbance attenuation increases with increasing batch period, as long as excitation persists over the longer batch period. Because of the dependence of disturbance attenuation on the excitation level, the batch ID algorithm must be switched off during periods of poor excitation.

If a state derivative measurement is not available (the FSI case), then an integrating prefilter can be used in a manner similar to the input and output prefiltering of Sastry & Bodson (1989). The essential concept arises from recognition that integrating both sides of (8) eliminates the state derivative, but requires the integration of the $A(x(t), v(t))$ and $b(x(t), v(t))$ terms. The prefilter is used to calculate the integral of these terms. Since a pure integration prefilter is only marginally stable, a prefilter with a slow, arbitrarily chosen pole at $-\lambda < 0$ is generally used. The prefilter is then described by

$$\dot{\bar{A}} = -\lambda\bar{A} + A(x(t), v(t)), \ \bar{A}_\circ = 0 \tag{12}$$

$$\dot{\bar{b}} = -\lambda\bar{b} + b(x(t), v(t)), \quad \bar{b}_\circ = x_\circ \tag{13}$$

where $\bar{A} \in I\!R^{n\times r}$ and $\bar{b} \in I\!R^n$ constitute the state of the prefilter. With this prefiltering, matrix least-squares is applied to the filtered system of equations

$$\bar{\mathcal{A}}\chi = X - \bar{\mathcal{B}} \tag{14}$$

where $\bar{\mathcal{A}}$, $\bar{\mathcal{B}}$, and X denote the concatenation of $\bar{A}(x_{t_i}, v_{t_i})$, $\bar{b}(x_{t_i}, v_{t_i})$, and $x(t_i)$, respectively. Hence the batch FSI algorithm is given by (12)–(13) and

$$\hat{\chi} = \left[\bar{\mathcal{A}}^T\bar{\mathcal{A}}\right]^{-1}\bar{\mathcal{A}}^T\left(X - \bar{\mathcal{B}}\right). \tag{15}$$

(Note that strictly speaking, this algorithm is no longer a batch algorithm, since the prefiltered information at any instant depends on its entire history. Nevertheless, it is an extension of the batch algorithm, and the misnomer is used.) In this case, the estimation error is given by

$$\tilde{\chi} = \left[\bar{\mathcal{A}}^T \bar{\mathcal{A}}\right]^{-1} \bar{\mathcal{A}}^T \overline{\mathcal{D}}_p \tag{16}$$

where $\overline{\mathcal{D}}_p$ is the concatenation of the prefiltered process noise. The FSI algorithm in (12)–(13) and (15) can also be used in the NPFSI case, by replacing x with the state measurement y. In this case the parameter estimation error expression is more complex, since now the measurement error d_m must be included.

3.2 Extended Kalman filter algorithm

The well-known Kalman filter algorithm provides a minimum-variance, unbiased state estimate for a linear system with uncorrelated white Gaussian process and measurement noise (Kalman & Bucy, 1961). Kalman filtering techniques can be applied directly to the parameter identification problem of (4)–(5) when FSDI information is available. This is done by treating χ as the state variable, using x and $\dot{x}$ as measurements, and estimating this "state" χ with the Kalman filter. The NPFSI identification problem of (4)–(5) can be cast into a state estimation problem by augmenting the state x of (4) with the parameters to be estimated and by using the differential equation $\dot{\chi} = 0$ to describe the evolution of χ. This results in the augmented system

$$\begin{bmatrix} \dot{x} \\ \dot{\chi} \end{bmatrix} = \begin{bmatrix} A(x,v)\chi + b(x,v) \\ 0 \end{bmatrix} + \begin{bmatrix} d_p \\ 0 \end{bmatrix} \tag{17}$$

$$y = \begin{bmatrix} I & 0 \end{bmatrix} \begin{bmatrix} x \\ \chi \end{bmatrix} + d_m \tag{18}$$

An estimate of the augmented state $z := \mathrm{col}(x, \chi)$ contains both a state estimate and a parameter estimate. Notice that even though the (nominal) system (4) is linear in this case, the augmented system (17)–(18) is nonlinear due to cross-product terms of x and χ, and hence an extended Kalman filter must be used. In general, the extended Kalman filter is a nonlinear state estimator whose filter gain is obtained by linearizing the system about some trajectory and then applying the (linear) Kalman filter to that linearized system (Sage & White, 1977). In this case, a closed-form expression for the linearization is available, and hence the system is linearized about the present (augmented-state) estimate $\hat{z} := \mathrm{col}(\hat{x}, \hat{\chi})$, yielding the algorithm

$$\dot{\hat{z}} = \begin{bmatrix} A(\hat{x},v)\hat{\chi} + b(\hat{x},v) \\ 0 \end{bmatrix} + \Sigma H^T R(t)^{-1} \left[y - H\hat{z}\right] \tag{19}$$

$$\dot{\Sigma} = D(\hat{z},v)\Sigma + \Sigma D(\hat{z},v)^T + P(t) - \Sigma H^T R(t)^{-1} H \Sigma \tag{20}$$

where $\Sigma(t) \in I\!R^{(n+r)\times(n+r)}$, $\Sigma(0) = Q_\circ > 0$, $H = [I \;\; 0]$, and

$$D(\hat{z},v) = \begin{bmatrix} \dfrac{\partial}{\partial \hat{x}} A(\hat{x},v)\hat{\chi} + \dfrac{\partial}{\partial \hat{x}} b(\hat{x},v) & 0 \\ A(\hat{x},v)^T & 0 \end{bmatrix}.$$

Note that while the Kalman gain evolution (20) is based on the linearization of the augmented-state system, the state estimate evolution (19) uses the original nonlinear dynamics.

When using a Kalman filter to estimate the state of a linear system, the choice of $P(t)$, $R(t)$, and $Q_\circ$ as the covariances of the process noise, measurement noise, and initial state, respectively, results in the a minimum-variance, unbiased estimate with the state estimate error covariance given by the solution $\Sigma(t)$ of (20). However, with the extended Kalman filter, this stochastic optimality is no longer forthcoming, hence $P(t)$, $R(t)$, and $Q_\circ$ are treated as algorithm design parameters to be chosen by the user. In this nonlinear setting, there is no general theory for choosing $P(t)$, $R(t)$, and $Q_\circ$ optimally, and $\Sigma(t)$ has no interpretation in terms of error variance. Furthermore, since the algorithm is based on a linearization about the estimated trajectory, the filter can suffer a divergence in the estimates if the state estimation error becomes too large. This divergent behavior is demonstrated for discrete-time systems by Ljung (1979).

3.3 H^∞ algorithms

The H^∞ approach to identification treats exogenous signals as deterministic but unknown quantities, and provides performance which is guaranteed over all such signals. This worst-case performance is a useful formulation when the unknown signals contain deterministic components (as in this case), or when they are random but with unknown statistics. In the FSDI case, Didinsky et al. (1995) have demonstrated that H^∞-based identification is a generalization of both LMS and RLS identification, and achieves a guaranteed disturbance attenuation level γ between the unknown quantities and the parameter estimate error. In this case, given any particular choice of the unknown quantities $d_p \in L_\infty(\mathbb{R}^n)$ and $\chi \in \mathbb{R}^r$, disturbance attenuation is defined to be the ratio

$$\frac{\|\chi - \hat{\chi}\|_{Q(x,v)}}{\sqrt{\|d_p\|^2 + |\chi - \hat{\chi}_\circ|^2_{Q_\circ}}} \tag{21}$$

where $\hat{\chi}_\circ$ is an *a priori* estimate of the parameter vector χ, $\|\cdot\|_Q$ is an L_2 semi-norm with a chosen weighting function $Q(x,v) \geq 0$, and $|\cdot|_{Q_\circ}$ is a generalized Euclidean norm $x^T Q_\circ x$ with chosen $Q_\circ > 0$. The FSDI H^∞ algorithm provides guaranteed performance in the sense that the ratio (21) is bounded by γ for all $d_p \in L_\infty(\mathbb{R}^n)$ and all $\chi \in \mathbb{R}^r$, so long as γ is larger than the minimum achievable disturbance attenuation level γ^*. (To be precise, γ^* may not be a minimum of the achievable disturbance attenuation levels, but may only be the greatest lower bound of such levels.) This is true whether d_p is generated by unmodeled or nonlinear dynamics, or is the sample path of a random process, so long as it belongs to $L_\infty(\mathbb{R}^n)$. The value of γ^* is problem dependent and may in some cases be ∞, meaning by convention that no guaranteed disturbance attenuation level can be achieved. However, the value of γ^* is also affected by the choice of Q, and if $Q(x,v)$ is chosen as $A(x,v)^T A(x,v)$ then $\gamma^* = 1$.

For any $\gamma \geq \gamma^*$ the FSDI identification algorithm as given by Didinsky et al. (1995) is

$$\dot{\hat{\chi}} = \Sigma^{-1} A(x,v)^T \left[\dot{x} - A(x,v)\hat{\chi} - b(x,v)\right] \tag{22}$$

$$\dot{\Sigma} = A(x,v)^T A(x,v) - \gamma^{-2} Q(x,u) \tag{23}$$

with initial conditions $\hat{\chi}(0) = \hat{\chi}_\circ$ and $\Sigma(0) = Q_\circ > 0$, and where $\hat{\chi}(t)$ is the estimate of the parameter χ and $\Sigma(t) \in \mathbb{R}^{r \times r}$. Note that when $\gamma \uparrow \infty$, the limiting filter is the RLS estimator. Also, when $Q(x,v)$ is chosen as $A(x,v)^T A(x,v)$ and $\gamma = \gamma^*$ $(= 1)$, the filter becomes a generalized LMS estimator.

To summarize: for a particular identification problem in the form of (4) with FSDI information available and with $A(x,v)$ and $b(x,v)$ known, design of the H^∞ algorithm consists of choosing the function $Q(x,v) \geq 0$, the matrix $Q_\circ > 0$ and the value $\gamma > \gamma^*$. The value of γ^* generally depends in a complicated fashion on A, b, $Q_\circ$, and Q, but is known to be 1 when Q is chosen as $Q = A^T A$. With these choices, the identifier given by (22)–(23) is guaranteed to provide a disturbance attenuation level γ for all $d_p \in L_\infty(\mathbb{R}^n)$ and all $\chi \in \mathbb{R}^r$.

In the NPFSI case, measurement noise is incorporated into the formulation. In particular, the guaranteed disturbance attenuation level becomes for $\gamma > \gamma^*$,

$$\frac{\|\chi - \hat{\chi}\|^2_{Q(x,v)}}{\|d_p\|^2 + \|d_m\|^2 + |\chi - \hat{\chi}_\circ|^2_{Q_\circ} + |x_\circ - \hat{x}_\circ|^2_{P_\circ}} \leq \gamma^2$$

for all $d_p, d_m \in L_\infty(\mathbb{R}^n)$, $\chi \in \mathbb{R}^n$ and $x_\circ \in \mathbb{R}^n$, where $P_\circ > 0$ is chosen by the user. Note that now both d_m and the initial state estimate error $x_\circ - \hat{x}_\circ$ are incorporated into the attenuation bound. Again, γ^* is not generally known and may be infinite.

The NPFSI algorithm for $\gamma \geq \gamma^*$ is

$$\begin{bmatrix} \dot{\hat{x}} \\ \dot{\hat{\chi}} \end{bmatrix} = \begin{bmatrix} 0 & A \\ 0 & 0 \end{bmatrix} \begin{bmatrix} \hat{x} \\ \hat{\chi} \end{bmatrix} + \begin{bmatrix} b \\ 0 \end{bmatrix} + \Sigma^{-1} \begin{bmatrix} I \\ 0 \end{bmatrix} (y - \hat{x}) \tag{24}$$

$$\dot{\Sigma} = -\Sigma \begin{bmatrix} 0 & A \\ 0 & 0 \end{bmatrix} - \begin{bmatrix} 0 & 0 \\ A^T & 0 \end{bmatrix} \Sigma + \begin{bmatrix} I & 0 \\ 0 & -\gamma^{-2} Q \end{bmatrix} - \Sigma \begin{bmatrix} I & 0 \\ 0 & 0 \end{bmatrix} \Sigma \tag{25}$$

where now $\Sigma(t) \in \mathbb{R}^{(n+r)\times(n+r)}$, with the initial condition $\Sigma(0) = \mathrm{diag}(P_\circ, Q_\circ)$. Notice that in (24)–(25) the dependence of A and b on (x,v) has been suppressed.

In the NPFSI case, the choice of $Q := A^T A$ does not yield $\gamma^* = 1$. In fact for the identification problem considered herein, it can be shown that $Q := A^T A$ yields infinite γ^*. To obtain a choice of Q which yields a known γ^* the following result of Didinsky et al. (1995) is used. For a given γ, if $\Sigma(t) > 0$ for all possible v, d_p, d_m, $x_\circ$, and χ, then $\gamma^* \leq \gamma$. Conversely, if for a particular γ there is some time t_1 and some (v, d_p, d_m, $x_\circ$, χ) for which $\Sigma(t_1) \not\geq 0$, then $\gamma^* > \gamma$.

This result can be used to specify an NPFSI algorithm with $\gamma^* = 1$. Using the partition

$$\Sigma =: \begin{bmatrix} \Sigma_1 & \Sigma_2 \\ \Sigma_2^T & \Sigma_3 \end{bmatrix}$$

with $\Sigma_1 \in \mathbb{R}^{n\times n}$, the Schur test for positivity states that $\Sigma(t) > 0$ if and only if $\Sigma_1(t) > 0$ and $\Pi(t) > 0$ where $\Pi := \Sigma_3 - \Sigma_2^T \Sigma_1^{-1} \Sigma_2$. Repeating the argument of Didinsky et al. (1995), from (25) it is easily shown that

$$\begin{aligned} \dot{\Sigma}_1 &= I - \Sigma_1 \Sigma_1, & \Sigma_1(0) &= P_\circ \\ \dot{\Pi} &= \Sigma_2^T \Sigma_2 - \gamma^{-2} Q, & \Pi(0) &= Q_\circ. \end{aligned}$$

Hence by choosing $P_\circ = I$ and $Q = \Sigma_2^T \Sigma_2$, $\gamma^* = 1$ is achieved for any $Q_\circ > 0$.

The H^∞ algorithm is superior to the previous algorithms in that it provides a guaranteed level of disturbance attenuation, regardless of the level of excitation and regardless of the statistical properties of the noise. Furthermore, Didinsky et al. (1995) give a persistency of excitation condition under which parameter estimates converge asymptotically to their true values in the presence of square-integrable disturbances d_p. Similar results are available neither for batch least-squares algorithms nor for extended Kalman filter identification. However, the H^∞ algorithm, as with the extended Kalman filter, does suffer from slow convergence under poor excitation.

4. Simulation results

Simulations of the three parameter ID algorithms were performed in order to evaluate the accuracy and timeliness of the parameter estimates. As described above, the baseline scenario for the simulation is a period of steady, level flight during which ice has accreted, followed by a maneuver. The maneuver is assumed to be an elevator doublet, *i.e.*, the input is one period of a sinusoid. For each algorithm, several doublets with amplitude varying from 1° to 10° and period varying from 5 s to 15 s were simulated. In the interest of brevity, simulation results are presented only for 1° and 5° elevator doublets over 10 s, with general comments made about the larger set of simulations.

As mentioned above, the process noise d_p is used to represent the higher-order terms f_u, f_w, and f_q in the flight dynamics as well as turbulence. The appropriate way to address the effect of higher-order terms in simulation is to apply the linear-model-based algorithms to a nonlinear model which includes these higher-order terms. Unfortunately, such a nonlinear model does not exist. Even though the recent literature has seen progress in the area of nearly globally accurate nonlinear flight dynamics models (see, for example, Morelli (1995)), there has yet to be a nonlinear model developed that incorporates the effects of icing. For this reason the nonlinear effects are not modeled.

In the simulations, both the turbulence and the measurement noise d_m are modeled as sample paths of zero-mean, bandlimited white Gaussian noise with bandwidth of 50 Hz. The bandwidth of the noise was chosen to be two orders of magnitude higher than the fastest modal frequency of the (known) flight dynamics, hence the effect of the bandlimited white noise will be essentially that of true white noise. Furthermore, both the measurement noise and process noise are assumed to have uncorrelated elements, and hence are completely characterized by their covariance matrix diagonals. For the measurement noise, these intensities are the NASA Twin Otter instrument resolution specifications, and are given in Table 2. Simulations were performed for light, moderate, and heavy turbulence levels, with noise intensities corresponding to $0.05g$, $0.2g$, and $0.4g$ of acceleration, respectively.

Table 2: Measurement noise intensities taken from NASA Twin Otter instrument resolution specifications as reported by Ratvasky & Ranaudo (1993).

σ_q	σ_θ	σ_α	σ_u
0.0167°/s	0.0293°	0.003°	0.039 m/s

In each case, $\chi := \mathrm{col}(M_\alpha, M_{\delta_E}, M_q, Z_\alpha, Z_{\delta_E}, Z_q, X_\alpha, X_u{+}X_{T_u})$ is estimated, but only the pitching moment derivatives M_α, M_{δ_E}, and M_q are considered for icing indication, as extensive simulation has shown that only these three parameters provide useful estimates. The Z parameters generally converge too slowly, and the X parameters are too sensitive to noise. The simulations begin with the doublet maneuver, and the arithmetic average of the iced and clean parameter values for each parameter is used as a threshold for rough evaluation and comparison of the algorithms. Both iced-aircraft and clean-aircraft simulations are performed. The iced-aircraft simulations investigate an accurate positive indication of icing, whereas the clean-aircraft simulations investigate an incorrect positive icing indication, or "false alarm".

It is also desirable to characterize the statistics of the parameter estimates. If the identification algorithms depended only linearly on the system state, then $\hat{\chi}$ would be a Gaussian random pro-

cess that could be characterized in terms of its mean and variance, as with the familiar Kalman filter (Kalman & Bucy, 1961). However, each of the algorithms being considered is nonlinear in the following sense: the equation describing the evolution of the parameter estimate involves either products of elements of x or cross-products of elements of x with elements of $\hat{\chi}$. This is true even without considering the unmodeled nonlinear dynamics. Because of this nonlinearity, the parameter estimate is not necessarily Gaussian, and the evolution of the mean and variance of $\hat{\chi}$ will involve higher-order statistics, as discussed in (Poor, 1994). In order to characterize the statistics of the parameter estimates, in each case multiple simulations were performed, each with different noise and turbulence sample paths.

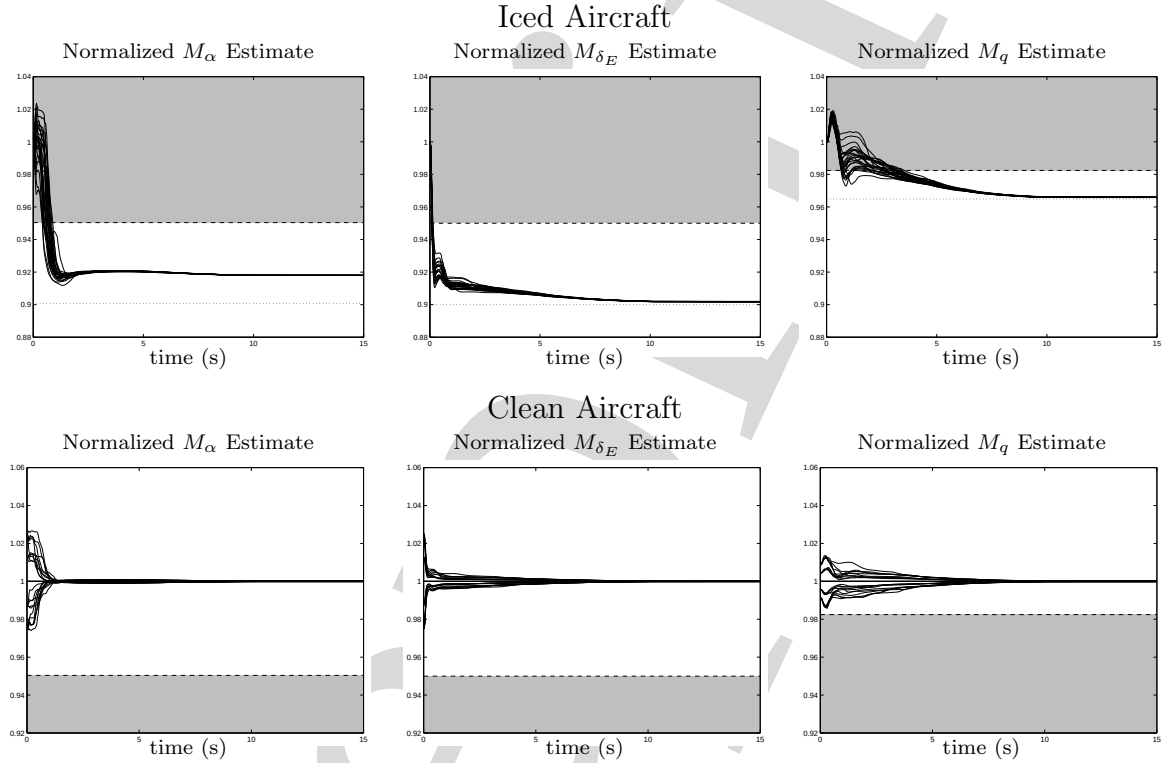

Figure 5: Simulation results for the H^∞ FSDI algorithm using a 5° doublet input and moderate turbulence. The algorithm used $\gamma = 3$, $Q = A^T A$, and $Q_\circ = (1 \times 10^{-6})I$. Normalized parameter estimates are plotted for both the clean and iced aircraft cases. In the clean case, estimates are shown for various initial parameter estimation errors, corresponding to different levels of trim point creep. For each case, 25 simulations have been performed, each for a different noise realization. The dashed line represents the simple detection threshold.

4.1 H^∞ simulations

The iced-aircraft simulations of the recursive H^∞ algorithms use the clean parameters as the initial parameter estimate $\hat{\chi}_\circ$ of (22). The clean-aircraft simulation, on the other hand, uses an initial parameter estimate that roughly represents the parameter variation *in the absence of ice* over the period of steady, level flight (*e.g.*, due to trim condition creep). Simulations were performed for

several initial estimate values, with the bounding value chosen as half of the distance from the clean value to the threshold. Both the FSDI and NPFSI H^∞ algorithms were simulated.

As seen in (22)–(23), the H^∞ FSDI algorithm is specified by the disturbance attenuation level $\gamma > \gamma^*$, the cost $Q(x, v)$, and the initial condition $Q_\circ$. $Q = A^T A$ has been chosen so that γ^* is known to be 1. Moreover, a value of $\gamma > \gamma^*$ is used (in this case $\gamma = 3$) since $\gamma = \gamma^*$ can result in a numerically sensitive algorithm. Furthermore, extensive simulation has determined that $Q_\circ = (1 \times 10^{-6})I$ gives a balance of fast convergence and noise insensitivity. Determination of this value was aided by the intuition that a larger value of $Q_\circ$ provides a larger initial condition for $\Sigma(t)$ in (23), which in turn results in a smaller "gain" $\Sigma^{-1}A(x, v)$ on the parameter estimate error term $\dot{x} - A(x, v)\hat{\chi} - b(x, v)$ in (22).

The simulation results for the FSDI H^∞ algorithm during the baseline maneuver with moderate turbulence are shown in Figure 5, where the parameter estimates, normalized by their clean values, for both the iced and clean simulations are plotted. Each plot in Figure 5 contains the results of 25 simulations run with various sample paths of the turbulence. In the plots, the dashed lines are the thresholds of the respective parameters, and the shaded area represents the side of the threshold that gives an incorrect icing indication. For the iced-aircraft, all three parameters move below the threshold within roughly 3 s, demonstrating that an accurate and unambiguous indication of icing would occur within that period for the baseline scenario. On the other hand, for the clean aircraft the parameter estimates never move below the threshold, indicating that a false alarm will not occur for the baseline scenario. The apparent bias in the M_α estimate is caused by poor excitation after the termination of the maneuver at 10 s, not by any inherent limitation of the algorithm. Simulation results of the H^∞ FSDI algorithm for input over several hundreds of seconds demonstrate that the M_α estimate converges toward the true value, as the theory predicts. (Of course, convergence in the limit can never be truly validated with the finiteness of numerical simulation.)

The simulation results for the NPFSI case during the baseline maneuver with moderate turbulence are shown in Figure 6. For the NPFSI algorithm in (24)–(25), Q, $Q_\circ$, $P_\circ$, and γ are available as design parameters, with the restriction that $\gamma > \gamma^*$. In order to obtain $\gamma^* = 1$, the values $P_\circ = I$ and $Q = \Sigma_2^T \Sigma_2$ were chosen. The value of γ was picked as 3, and extensive simulation determined that the value $Q_\circ = (1 \times 10^{-7})I$ was appropriate. Here again, the intuitive understanding that larger $Q_\circ$ yields smaller "gain" $\Sigma^{-1}(t)$ was used. For the NPFSI algorithm, the addition of noise degraded the accuracy of the parameter estimates. In particular, the M_q estimates for the clean aircraft registered a false alarm for certain noise sample paths for all initial estimate errors. However, the M_{δ_E} and M_α estimates still yield icing indications within 3 s without false alarm. The results are nearly as promising for input doublets down to 1° amplitude, shown in Figure 7. The minimal effect of turbulence level on algorithm performance is clear from Figure 8, where parameter estimates are shown for the iced aircraft under light, moderate, and heavy turbulence. From these results, as well as a comparison of the moderate turbulence NPFSI and FSDI results, it is clear that measurement noise rather than turbulence dominates the parameter estimate error.

4.2 Extended Kalman filter simulations

As with the H^∞ algorithms, the extended Kalman filter algorithm is recursive, and hence depends on an initial parameter estimate. Simulations for the EKF algorithm were performed for both clean and iced aircraft with initial conditions as in the H^∞ simulations. Although the EKF algorithm can be used for either the FSDI case or the NPFSI case, results are presented only for the NPFSI

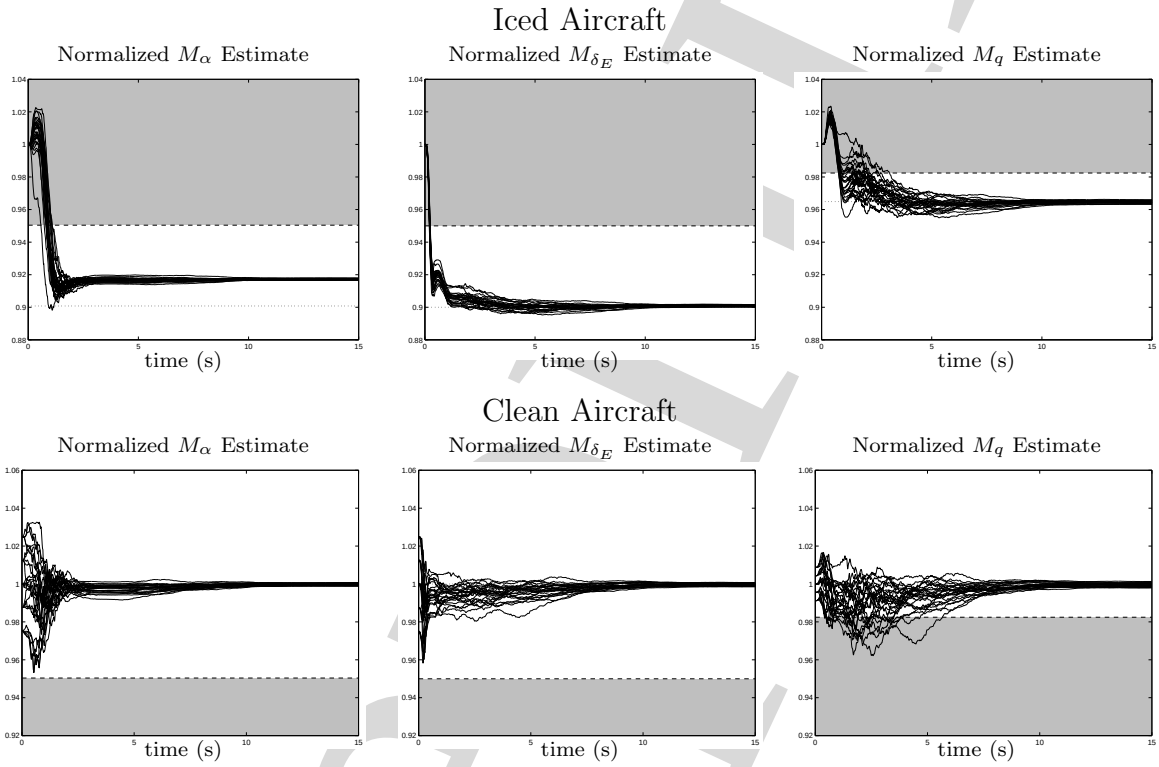

Figure 6: Simulation results for the H^∞ NPFSI algorithm using a 5° doublet input and moderate turbulence. The algorithm used $\gamma = 3$, $Q = \Sigma_2^T \Sigma_2$, and $Q_\circ = (1 \times 10^{-7})I$. Normalized parameter estimates are plotted for both the clean and iced aircraft cases. In the clean case, estimates are shown for various initial parameter estimation errors, corresponding to different levels of trim point creep. For each case, 25 simulations have been performed, each for a different noise realization. The dashed line represents the simple detection threshold.

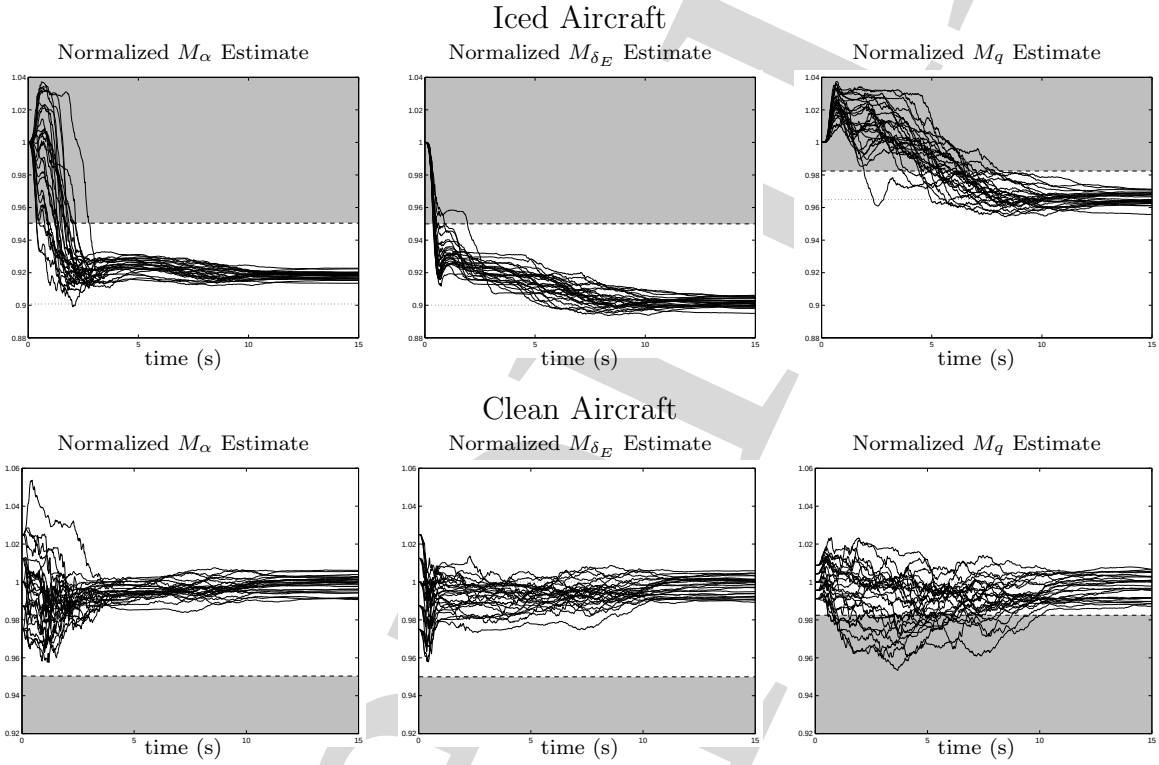

Figure 7: Simulation results for the H^∞ NPFSI algorithm using a 1° doublet input and moderate turbulence. The algorithm used $\gamma = 3$, $Q = \Sigma_2^T \Sigma_2$, and $Q_\circ = (1 \times 10^{-7})I$. Normalized parameter estimates are plotted for both the clean and iced aircraft cases. In the clean case, estimates are shown for various initial parameter estimation errors, corresponding to different levels of trim point creep. For each case, 25 simulations have been performed, each for a different noise realization. The dashed line represents the simple detection threshold.

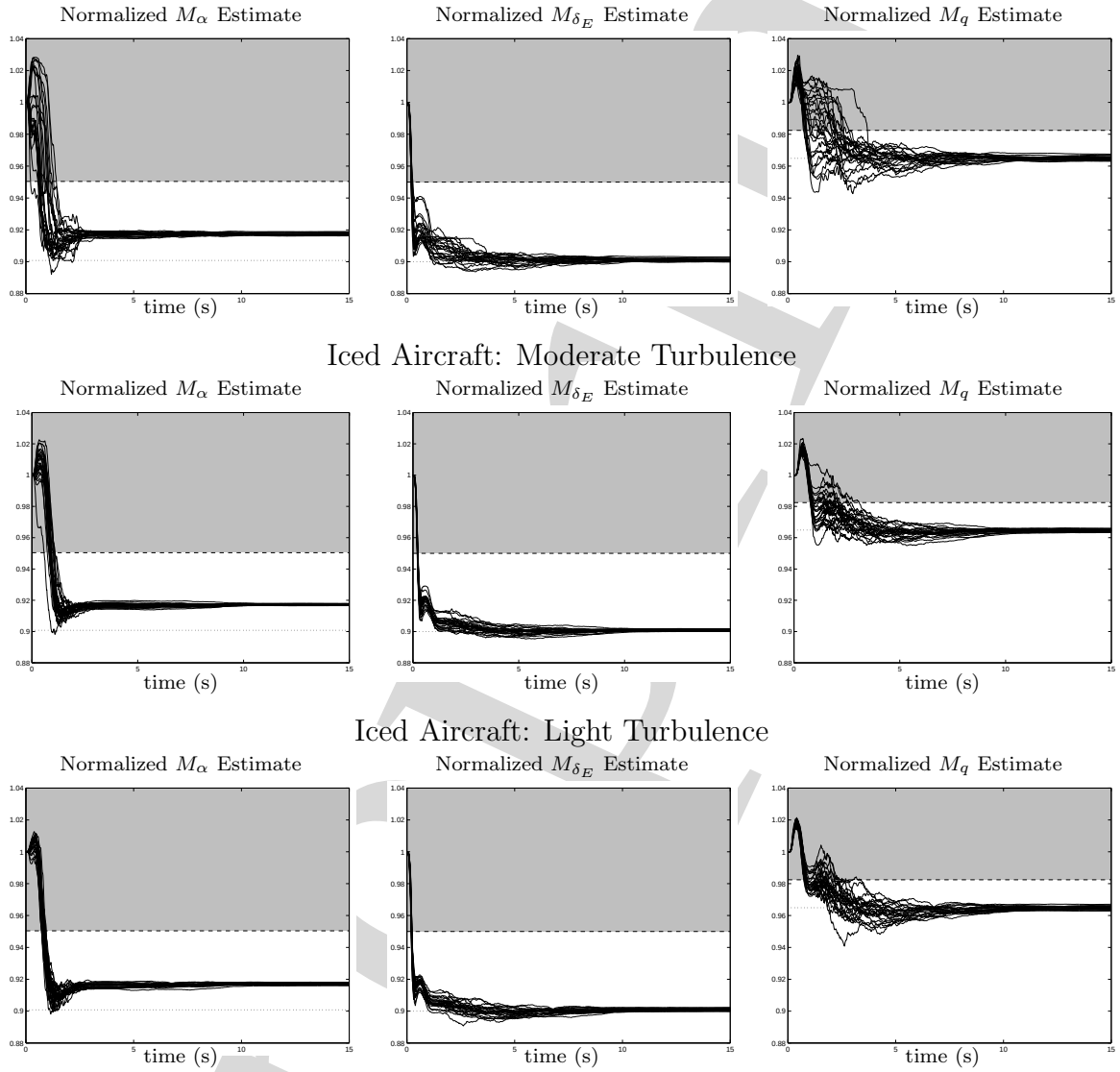

Figure 8: Comparison of simulation results for the H^∞ NPFSI algorithm for light, moderate, and heavy turbulence. Results are for an iced aircraft and a 5° doublet input was used. The algorithm used $\gamma = 3$, $Q = \Sigma_2^T \Sigma_2$, and $Q_\circ = (1 \times 10^{-7})I$. For each case, 25 simulations have been performed, each for a different noise realization. The dashed line represents the simple detection threshold.

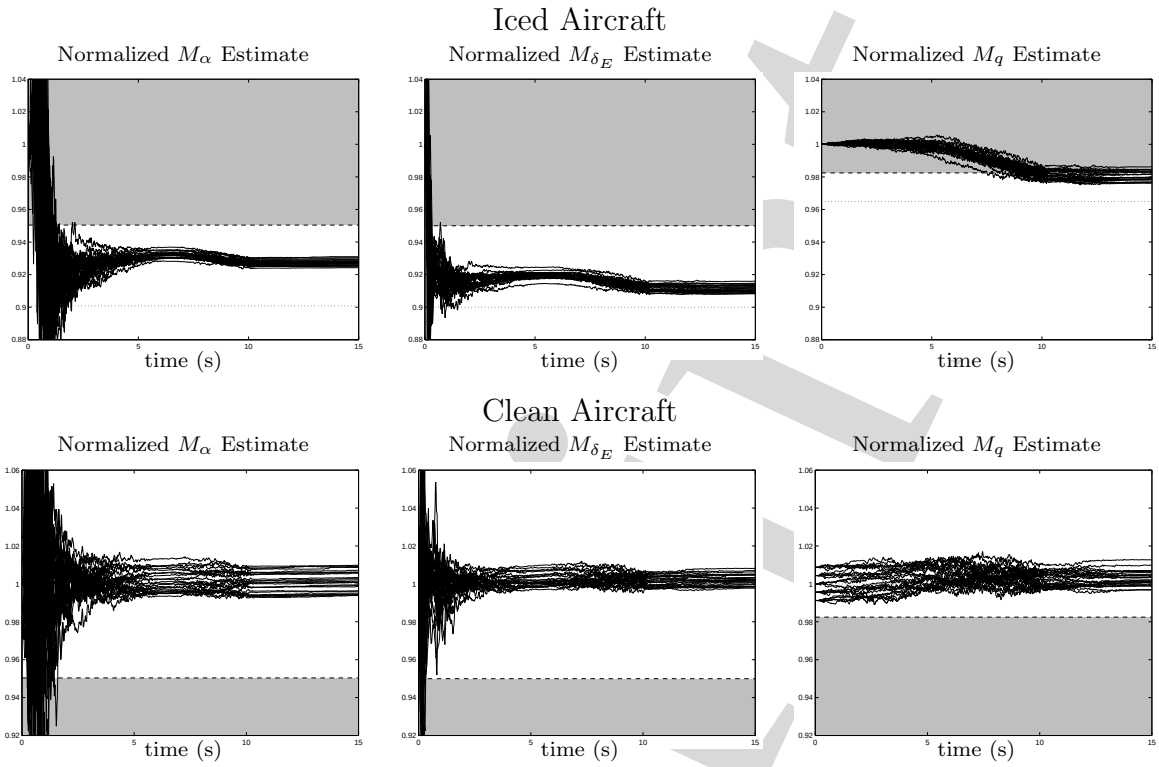

Figure 9: Simulation results for the EKF algorithm with process noise and measurement noise using a 5° doublet input and moderate turbulence. The algorithm used $P(t) \equiv 0.1I$, $R(t) \equiv (1 \times 10^{-5})I$, and $Q_\circ = (1 \times 10^4)I$. Normalized parameter estimates are plotted for both the clean and iced aircraft cases. In the clean case, estimates are shown for various initial parameter estimation errors, corresponding to different levels of trim point creep. In each case, the dashed line represents the simple detection threshold.

case.

The simulation results are shown in Figure 9. Much experimentation resulted in a choice of $P(t) \equiv 0.1I$, $R(t) \equiv (1 \times 10^{-5})I$ and $Q_\circ = (1 \times 10^4)I$, where the algorithm performance was judged based on timeliness and accuracy. Determination of the best values for $R(t)$, $P(t)$, and $Q_\circ$ was difficult and time consuming, since the relation between these matrices and the performance was complex and coupled. The authors' efforts consisted essentially of trial and error. As seen in Figure 9, the EKF algorithm was unable to provide a timely indication of icing without false alarm for most cases. The M_q estimates are completely useless, and the M_{δ_E} and M_α estimates contain wild transients that yield false alarms. The results for less excitation, shown in Figure 10, were much worse, with the large transients dominating the estimates for the first 3 to 5 s. One might argue that a reliable indication of icing could be obtained ignoring the first several seconds of the M_{δ_E} and M_α estimates, then basing the indication on the subsequent value of the estimates. However, since the period of dominance of the transient is inversely related to the level of excitation, this scheme would be unreliable. The poorer transient performance of the extended Kalman filter is consistent with the fact that there is no guaranteed disturbance attenuation bound as for the H^∞ algorithm.

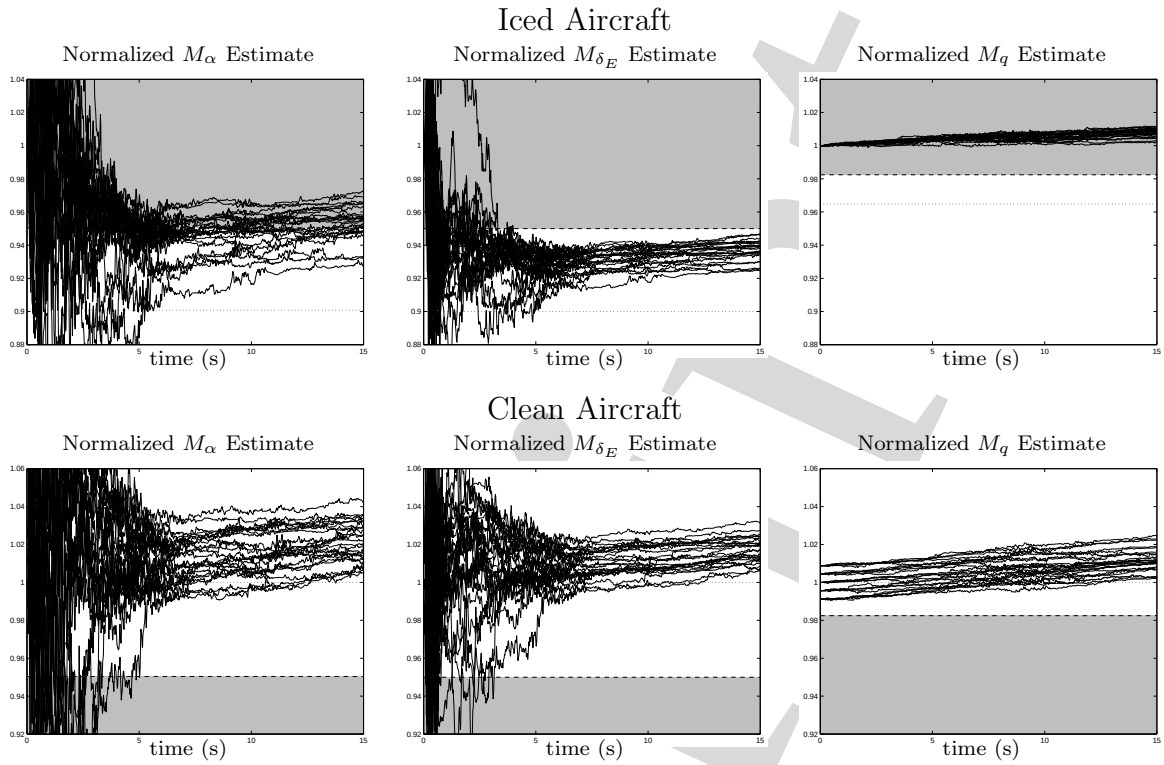

Figure 10: Simulation results for the EKF algorithm with process noise and measurement noise using a 1° doublet input and moderate turbulence. The algorithm used $P(t) \equiv 0.1I$, $R(t) \equiv (1 \times 10^{-5})I$, and $Q_\circ = (1 \times 10^4)I$. Normalized parameter estimates are plotted for both the clean and iced aircraft cases. In the clean case, estimates are shown for various initial parameter estimation errors, corresponding to different levels of trim point creep. In each case, the dashed line represents the simple detection threshold.

4.3 Batch least-squares simulations

Since the batch least-squares algorithm is static, there are no initial parameter estimates. The batch algorithm was implemented as a sliding batch window, yielding a new estimate at every sample instant calculated from information available at the previous m sample instants according to (10). A sample rate of 30 Hz was used.

Results of the clean-aircraft and iced-aircraft simulations of the batch FSDI algorithm are shown in Figure 11. A batch period of 8 s was chosen. Clearly the parameter estimates are useless for icing detection. This was the case for any reasonable batch period. If the noise is substantially reduced (by a factor of 10 in intensity), the algorithm provides an accurate icing indication in several seconds without false alarm after that period. Similarly, simulation results have shown that drastically increased excitation levels ($\sim 50°$ doublets) provide timely and unambiguous icing indication, although this is only of academic interest as a 50° doublet is both not available and not meaningful in a linearized flight dynamics setting. As would be expected, the FSI and NPFSI simulation results were worse than the FSDI results. For the sake of brevity, these results are not included.

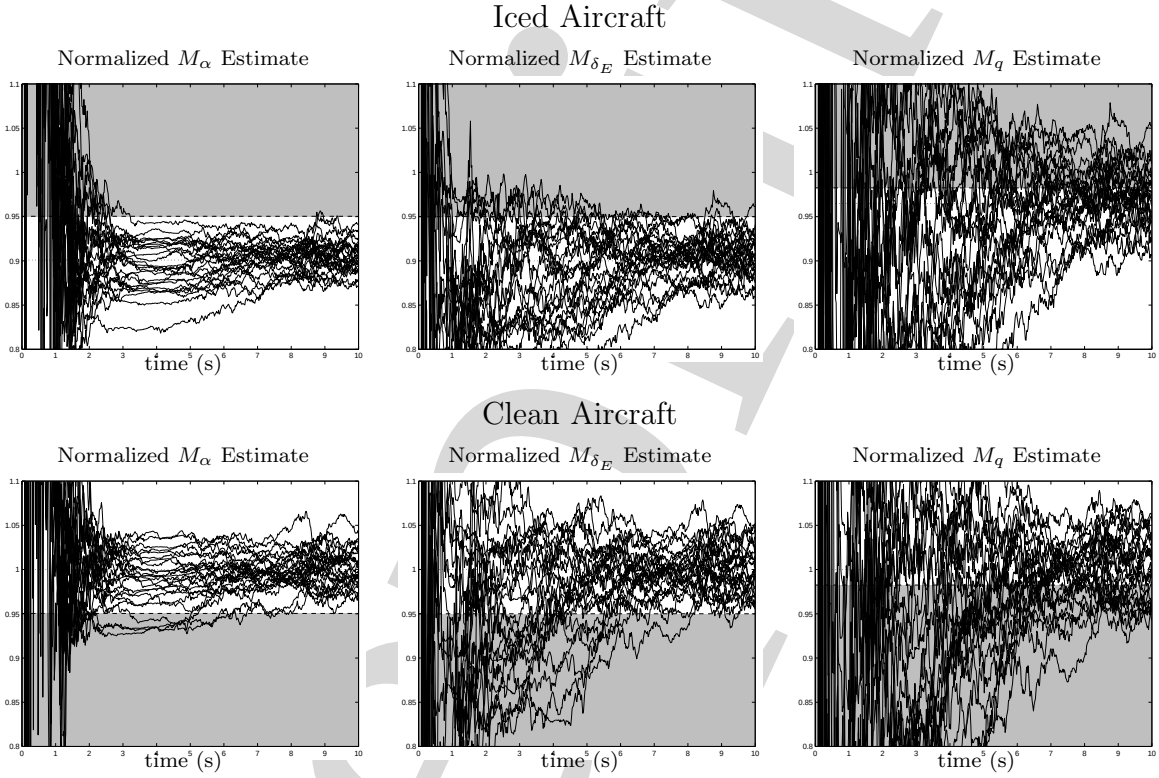

Figure 11: Simulation results for batch least-squares FSDI algorithm using a 5° doublet input and moderate turbulence. The algorithm used a batch period of 8 s. Normalized parameter estimates are plotted for both the clean and iced aircraft cases. In each case, the dashed line represents the simple detection threshold.

5. Conclusion

This study has investigated the performance of a batch least-squares ID algorithm, an extended Kalman filter, and H^∞ ID algorithms in the context of icing detection. A period of steady, level flight followed by a doublet maneuver has been used as a baseline flight scenario, where the identification begins with the maneuver. Iced and clean aircraft models based on the NASA Twin Otter inflight icing research aircraft have been used with the typical linearization about a trim condition. The actual flight dynamics parameters were assumed constant during the maneuver. The icing detection was modeled as a simple detection threshold for each parameter, with the threshold being the mean of the iced and clean parameters. Simulations for the iced and clean aircraft have been performed in order to investigate both accurate icing indications and false alarms. The simulation results demonstrate that accurate and unambiguous icing indications are available in 3 s for the H^∞ algorithm in the presence of measurement noise, for the given baseline scenario. The extended Kalman filter algorithm yields ambiguous results for all parameters for smaller excitation levels, and the batch results do not contain any meaningful information for any reasonable level of excitation. The inferior performances of the batch algorithm and the extended Kalman filter are consistent with the lack of a guaranteed disturbance attenuation bound with these algorithms, whereas with the H^∞ algorithms such a guaranteed bound does exist.

As a continuation of this work, the authors plan to study identification during steady, level flight where the assumed time-invariance of the parameters is no longer valid and where the excitation is provided only by turbulence. In this case, parameter convergence is expected to be much slower; however, detection need not be as timely since a handling event would not be imminent without a maneuver. As mentioned above, preliminary results have been obtained by Hillbrand (1999) along these lines. Furthermore, the preliminary ice detection and characterization work of Schuchard et al. (2000) should be extended to a more sophisticated characterization that incorporates other available information, such as drag and lift coefficient estimates, hinge moment estimates, ice sensor measurements, and local aerodynamic measurements. In particular, the problem formulation contained herein suffers from its dependence on the trim condition, or linearization operating point. Although the linearization is a valid simplification for the small-excursion maneuvers considered, the icing detection must take into account the expected clean-aircraft parameters at the trim point. These parameters are functions of the trim condition, and this variability may make implementation difficult by requiring large look-up tables in the detection algorithm. A simplifying formulation may be to view the identification problem in a full nonlinear setting, and to identify some parameterization of the aerodynamic forces and moments. This formulation would further lend itself to investigation of control adaptation during handling icing events, where large excursions make the linearization assumption invalid.

6. Acknowledgments

This work was supported in part by NASA, and in part by the University of Illinois at Urbana-Champaign under the Critical Research Initiatives Program. The authors would like to credit Eric Keller, Wen Li, and Eduardo Salvador for their implementation and simulation of the various identification algorithms involved here. Furthermore, the authors thank Michael Bragg for providing his expertise in aircraft icing in general and in ice accretion in particular.

References

Åström, K. J. & Wittenmark, B. (1995). *Adaptive Control*, 2^{nd} edn, New York, NY: Addison-Wesley.

Bragg, M. B. (1996). Aircraft aerodynamic effects due to large droplet ice accretions. *Proc. 34^{th} AIAA Aerospace Sciences Meeting and Exhibit*, number AIAA–96–0932. Reno, NV.

Bragg, M. B., Perkins, W. R., Sarter, N. B., Başar, T., Voulgaris, P. G., Gurbacki, H. M., Melody, J. W. & McCray, S. A. (1998). An interdisciplinary approach to inflight aircraft icing safety. *Proc. 36^{th} AIAA Aerospace Sciences Meeting and Exhibit*, number AIAA–98–0095. Reno, NV.

Chandler, P. R., Pachter, M. & Mears, M. (1995). System identification for adaptive and reconfigurable control. *AIAA Journal of Guidance, Control, & Dynamics 18*(3), 516–524.

Cole, J. & Sands, W. (1991). Statistical study of aircraft icing accidents. *Proc. 29^{th} AIAA Aerospace Sciences Meeting and Exhibit*, number AIAA–91–0558. Reno, NV.

Didinsky, G., Pan, Z. & Başar, T. (1995). Parameter identification of uncertain plants using H^{∞} methods. *Automatica 31*(9), 1227–1250.

Etkin, B. & Reid, L. D. (1996). *Dynamics of Flight: Stability and Control*, 3^{rd} edn, New York, NY: John Wiley and Sons.

Hillbrand, T. (1999). Identification of time-varying flight dynamics parameters for aircraft icing detection and classification using H^{∞} methods. *Technical Report UILU–ENG–99–2223 DC–190*, Coordinated Science Laboratory, University of Illinois at Urbana-Champaign.

Kalman, R. E. & Bucy, R. S. (1961). New results in linear filtering and prediction theory. *ASME Journal of Basic Engineering Series 83D*, 95–108.

Khalil, H. K. (1996). *Nonlinear Systems*, 2^{nd} edn, Upper Saddle River, NJ: Prentice-Hall.

Lee, S. & Bragg, M. B. (1999). Experimental investigation of simulated large-droplet ice shapes on airfoil aerodynamics. *Journal of Aircraft 36*(5), 844–850.

Ljung, L. (1979). Asymptotic behavior of the extended Kalman filter as a parameter estimator for linear systems. *IEEE Transactions on Automatic Control AC–24*(1), 36–50.

Ljung, L. (1999). *System Identification: Theory for the User*, Information and Systems Sciences Series, 2^{nd} edn, Englewood Cliffs, NJ: Prentice-Hall.

Morelli, E. A. (1995). Global nonlinear aerodynamic modeling using multivariate orthogonal functions. *Journal of Aircraft 32*(2), 270–277.

Murray, R. M., Sastry, S. S. & Li, Z. (1994). *A Mathematical Introduction to Robotic Manipulation*, Ann Arbor, MI: CRC Press.

NAS (1997). Weather investment recommendations. *Technical report*, NASA Aeronautics Safety Investment Strategy.

Olsen, W. & Shaw, R. (1984). Ice shapes and the resulting drag increase for a NACA 0012 airfoil. *Technical Report 83556*, NASA.

Poor, H. V. (1994). *An Introduction to Signal Detection and Estimation*, 2^{nd} edn, New York, NY: Springer-Verlag.

Ratvasky, T. P. & Ranaudo, R. J. (1993). Icing effects on aircraft stability and control determined from flight data. *Proc. 31st AIAA Aerospace Sciences Meeting and Exhibit*, number AIAA–93–0398. Reno, NV.

Ratvasky, T. P., Van Zante, J. F. & Riley, J. T. (1999). NASA/FAA tailplane icing program overview. *Proc. 37th AIAA Aerospace Sciences Meeting and Exhibit*, number AIAA–99–0370. Reno, NV.

Roskam, J. (1982). *Airplane Flight Dynamics and Automatic Flight Controls*, 2^{nd} edn, Ottawa, KS: Roskam Aviation and Engineering Corporation.

Sage, A. P. & White, III, C. C. (1977). *Optimum Systems Control*, 2^{nd} edn, Englewood Cliffs, NJ: Prentice-Hall.

Sastry, S. S. & Bodson, M. (1989). *Adaptive Control: Stability, Convergence and Robustness*, Information and System Sciences, Englewood Cliffs, NJ: Prentice-Hall.

Schuchard, E. A., Melody, J. W., Başar, T., Perkins, W. R. & Voulgaris, P. (2000). Detection and classification of aircraft icing using neural networks. *Proc. 38th AIAA Aerospace Sciences Meeting and Exhibit*, number AIAA–2000–0361. Reno, NV.

Stevens, B. L. & Lewis, F. L. (1992). *Aircraft Control and Simulation*, New York, NY: John Wiley and Sons.

Ward, D. G. & Barron, R. (1995). A self-designing receding horizon optimal flight controller. *Proc. 1995 American Control Conference*, (pp. 3490–3494). Seattle, WA.